Electron tunneling in biology: When does it matter? Supplementary Material

Setare M. Sarhangi[1] and Dmitry V. Matyushov[1]
School of Molecular Sciences and Department of Physics, Arizona State University, PO Box 871504, Tempe, AZ 85287-1504[a)]

I. SIMULATION PROTOCOLS

The X-ray diffraction structure (resolution 2.70 Å) of *Pseudomonas aeruginosa* azurin (PaAz, PDB 1AZU[?]) was adopted as the starting configuration for Molecular Dynamic (MD) simulations. The initial setup of the simulations for reduced (Red) and oxidized (Ox) states of azurin are created according to the simulation protocol described in detailed elsewhere.[1]

The tyrosine residue was replaced by the only tryptophan (res. No. 48) of azurin through applying patches using psfgen to create $\mathrm{Tyr}^{+}-\mathrm{Cu}^{\mathrm{I}}$ and $\mathrm{Tyr}-\mathrm{Cu}^{\mathrm{II}}$ states. The $\mathrm{Tyr}^{+}-\mathrm{Cu}^{\mathrm{I}}$ state of tyrosine was created by replacing tryptophan with positive tyrosine in the Red state of the azurin. The $\mathrm{Tyr}-\mathrm{Cu}^{\mathrm{II}}$ state of tyrosine was created by replacing tryptophan with tyrosine in the Ox state of the azurin. In the next step, 36469 TIP3P water molecules were added to the simulation box using the CHARMM force field and *solvate* plugin from VMD.[2] The size of the simulation box is 105 Å×105 Å×105 Å, consisting of the total of 111275 atoms. The total charge of the system in both states is $Q=-2$.

A new state with half charge for tyrosine and active site was created by applying a charge patch on the Red state of azurin according to the following charge rule: $\tilde{q}_j^D = q_j^D + \frac{1}{2}\Delta q_j^D$ and $\tilde{q}_j^A = q_j^A + \frac{1}{2}\Delta q_j^A$ where D is the electron donor (the active site) and A is the electron acceptor (tyrosine). The charges Δq_j are the differences of atomic charge between the final and initial states of the electron-transfer reaction (reaction scheme in Eq. 13 in the main text). The half-charge state was created to more efficiently sample the configurations near the crossing of the free-energy surfaces as explained below.

For all initial systems, steepest descent minimizations were performed for 250000 steps. The NPT equilibration simulation was done using the Langevin dynamics in NAMD with the following parameters: a damping coefficient of 1 ps^{-1}, the piston period of 100 fs, the piston decay time of 50 fs, the piston target pressure of 1.01325 bar, and constant temperature control set to the target temperature of 300 K. The NPT simulations with the length of 10 ns were performed for all states of protein. The stability of the protein structure was monitored through RMSD of the protein and the active site. The production NVT simulations were performed using the same parameters as the NPT simulations, but removing the constant pressure controls. Long-range electrostatic interactions were handled with the particle mesh Ewald technique using a cutoff distance of 12.0 Å. The time step of 2.0 fs was used for all simulations unless otherwise specified. All simulations were performed using NAMD software program[3]. 300 ns MD simulations were performed for trajectoires production in all states.

II. ATOMIC CHARGES OF TYROSINE

To produce the charge distribution of positive tyrosine, an isolated tyrosine residue was terminated with two alanines. The Gaussian16[4] package was then used to optimize the structure of the alanine-tyrsoine-alanine peptide (Ala-Tyr-Ala) with DFT/B3LYP and 6-31++g(d,p) basis set. The charge distribution of the positive tyrosine was calculated using Constrained Density Functional Theory (CDFT)[5] and B3LYP functional with four basis sets: 6-31G, 6-31+G∗, 6-311+G∗ and 6-311++G∗∗. For all charge calculations CHarges from ELectrostatic Potentials using a Grid-based method (CHELPG)[6] charge model(algorithm) was used. The constrained electronic structure calculations were performed with Q-Chem 5.4 package[7]. In the alanine-tyrsoine-alanine peptide, the tyrsoine and alanines were constrained to have positive and neutral charges, respectively. The resulting partial charges are listed in the table S1. The charges with basis sets 6-31G is used in simulation of $\mathrm{Tyr}^{+}-\mathrm{Cu}^{\mathrm{I}}$ state.

III. DYNAMICS OF THE STOKES SHIFT AND DISTANCE

MD simulations (10 ns) with a saving frequency of 5 fs were performed to study the short dynamic (for the Stokes-shift and donor-acceptor distance dynamics). The time step and saving frequency time are 1 fs and 5 fs, respectively. The Stokes-shift dynamics were monitored by the time auto-correlation function of the energy gap

$$C_X^{(i)}(t) = \langle \delta X(t)\delta X(0)\rangle_i. \tag{S1}$$

The normalized correlation function was fitted to four decaying exponents

$$S_2^{(i)}(t) = C_X^{(i)}(t)/C_X^{(i)}(0) = \sum_{n=1}^{4} A_n \exp^{-t/\tau_n}. \tag{S2}$$

The results of the fits for $\mathrm{Tyr}^{+}-\mathrm{Cu}^{\mathrm{I}}$ ($i=1$) and $\mathrm{Tyr}-\mathrm{Cu}^{\mathrm{II}}$ ($i=2$) states of azurin are shown in Figure S1. The fitting parameters are listed in Table S2.

a)Electronic mail: dmitrym@asu.edu

Table S1. Atomic charges of positive tyrosine calcualted from CDFT with four basis set 6-31G, 6-31+G*, 6-311+G* and 6-311++G** (CHELPG charge model).

Atom	6-31G	6-31+G*	6-311+G*	6-311++G**
N	-0.686685	-0.682691	-0.698381	-0.666612
HN	0.343448	0.329879	0.335752	0.321739
CA	0.463074	0.5614	0.570401	0.547402
HA	0.023292	-4.6e-05	0.001821	0.005039
CB	-0.344495	-0.414579	-0.43992	-0.433911
C	0.601551	0.47179	0.478744	0.469764
HB1	0.189713	0.195683	0.203423	0.202033
HB2	0.124484	0.128003	0.138069	0.137828
CG	0.211732	0.309715	0.307054	0.299014
O	-0.503963	-0.456653	-0.462068	-0.454008
CD2	-0.06088	-0.078685	-0.082261	-0.068831
CD1	-0.15534	-0.208224	-0.201688	-0.194307
HD2	0.166068	0.163261	0.169855	0.163487
CE2	-0.300065	-0.288419	-0.304326	-0.302888
CE1	-0.201827	-0.151434	-0.179032	-0.167266
HD1	0.18107	0.187202	0.190192	0.185475
HE2	0.200418	0.204283	0.20991	0.207679
CZ	0.593796	0.514799	0.541185	0.526196
HE1	0.205925	0.202859	0.212627	0.20574
OH	-0.547864	-0.473551	-0.491557	-0.466316
HH	0.501025	0.462812	0.473949	0.455066
$\sum \Delta q$	1.00	0.98	0.97	0.97

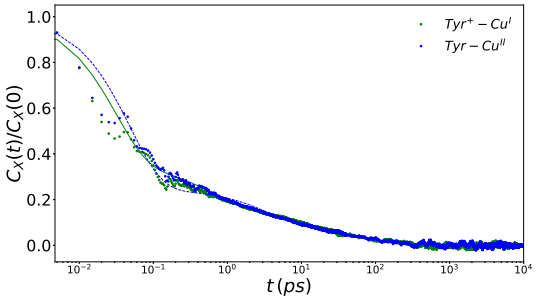

Figure S1. Correlation functions $C_X^{(i)}(t)/C_X^{(i)}(0)$ (points) calculated from Eq. (S1) and fitted to Eq. (S2) (lines) for $\mathrm{Tyr}^+ - \mathrm{Cu}^{\mathrm{I}}$ (green) and $\mathrm{Tyr} - \mathrm{Cu}^{\mathrm{II}}$ (blue) states.

The dynamics of distance between the center of mass of tyrosine's phenol ring and the copper atom of the active site were studied with the time correlation function

$$C_R^{(i)}(t) = \langle \delta R(t) \delta R(0) \rangle_i \tag{S3}$$

calculated for $\mathrm{Tyr} - \mathrm{Cu}^{\mathrm{II}}$ and $\mathrm{Tyr}^+ - \mathrm{Cu}^{\mathrm{I}}$ states. The correlation functions (points, Eq. (S3)) and their fits to Eq. (S4) are shown in Figure S2 for $\mathrm{Tyr}^+ - \mathrm{Cu}^{\mathrm{I}}$ and $\mathrm{Tyr} - \mathrm{Cu}^{\mathrm{II}}$ states. To reproduce the oscillation of the normalized correlation functions $C_R^{(i)}(t)/C_R^{(i)}(0)$, equation (S4) was used

$$\begin{aligned}\Phi(t) = {} & A \exp^{-\alpha t} + B \exp^{-\alpha_2 t} \sin \omega_1 t \\ & + (1 - A) \exp^{-\alpha_3 t} [\cos \omega_2 t + (\alpha_3/\omega_2) \sin \omega_2 t].\end{aligned} \tag{S4}$$

Table S2. The fitting parameters for the time correlation functions of the energy gap (Eq. (S2)). The average relaxation time τ_X and exponential relaxation times τ_i are in ps.

State	A_1	A_2	A_3	τ_1	τ_2	τ_3	τ_4	τ_X
$\mathrm{Tyr}^+ - \mathrm{Cu}^{\mathrm{I}}$	0.69	0.14	0.10	0.03	0.76	11.79	118.51	8.47
$\mathrm{Tyr} - \mathrm{Cu}^{\mathrm{II}}$	0.75	0.15	0.07	0.05	3.58	57.10	366.84	10.39

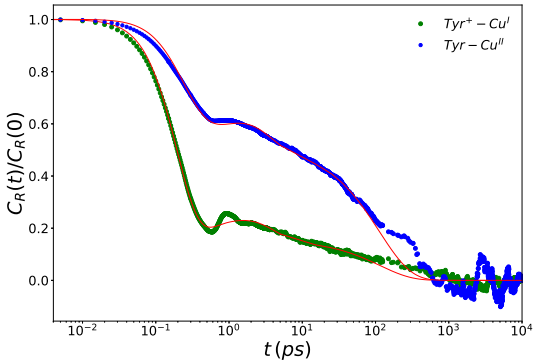

Figure S2. Correlation functions $C_R^{(i)}(t)/C_R^{(i)}(0)$ (points, Eq. (S3)) are fitted to Eq. (S4) (lines) for $\mathrm{Tyr}^+ - \mathrm{Cu}^{\mathrm{I}}$ (green) and $\mathrm{Tyr} - \mathrm{Cu}^{\mathrm{II}}$ (blue) states.

The fitting parameters are listed in Table S3.

The average distance between the copper atom of the active site and the center of mass of tyrosine's phenol ring are calculated along 300 ns of MD trajectories and are listed in Table S4. The distributions of distances R are shown in Figure S3.

IV. ELECTRON-TRANSFER ENERGY GAP

The electron-transfer energy gap is calculated by subtracting atomic charges of the donor and acceptor interacting with the electrostatic potential of the protein-

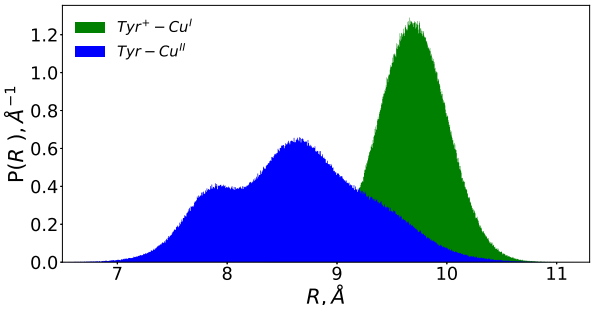

Figure S3. Distributions of distances between the Cu atom of the active site and the tyrosine's phenol ring in the initial, $\mathrm{Tyr}^+ - \mathrm{Cu}^{\mathrm{I}}$ (green), and final, $\mathrm{Tyr} - \mathrm{Cu}^{\mathrm{II}}$ (blue), electron-transfer states.

Table S3. The fitting parameters (Eq. (S4)) for the time correlation functions of the distance between the center of mass tyrosine's phenol ring and the copper atom of the active site. The relaxation time τ_R (ps) is the integral relaxation time.

State	A	B	α_1	α_2	α_3	ω_1	ω_2	$\langle\tau\rangle$
$\mathrm{Tyr}^+ - \mathrm{Cu}^{\mathrm{I}}$	0.16	455.52	0.009	0.62	8.50	4.90	0.0003	18.26
$\mathrm{Tyr} - \mathrm{Cu}^{\mathrm{II}}$	0.51	2014.03	0.009	0.69	7.97	-7.67×10^{-6}	0.00009	57.98

Table S4. Average distance between center of mass of tyrosine's phenol ring and the copper atom of the active site.

State	$\langle R\rangle$, Å
$\mathrm{Tyr}^+ - \mathrm{Cu}^{\mathrm{I}}$	9.69
$\mathrm{Tyr} - \mathrm{Cu}^{\mathrm{II}}$	8.63

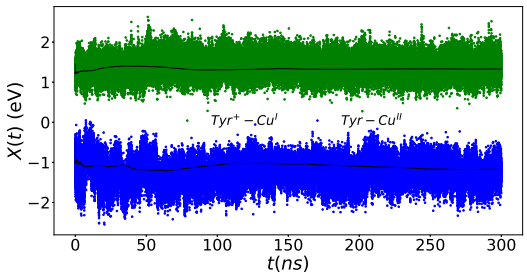

Figure S4. Energy gap $X(t)$ vs time for $\mathrm{Tyr}^+ - \mathrm{Cu}^{\mathrm{I}}$ (green) and $\mathrm{Tyr} - \mathrm{Cu}^{\mathrm{II}}$ (blue) states at 300 K. The black lines are the accumulated averages of the energy gap.

water thermal bath in final and initial electron-transfer states.[8,9]

$$X = E_2 - E_1 = \sum_j \Delta q_j^D \phi_j^D + \sum_j \Delta q_j^A \phi_j^A, \qquad \text{(S5)}$$

where $\Delta q_j^D = q_j^{D+} - q_j^D$ and $\Delta q_j^A = q_j^A - q_j^{A+}$ ($\sum_j \Delta q_j^D = +1$ and $\sum_j \Delta q_j^A = -1$). The PSF file with charges Δq_j for tyrosine and azurin's active site were created to calculate electrostatic interactions with water and protein. The electrostatic interaction was calculated by using the *namdenergy* plugin with replacing the partial charges of the active site and tyrosine by the differnce charges, Δq_j^A and Δq_j^D, respectively. Figure S4 shows the the targectories of $X(t)$ which sre used to calcualte the statistics. Figure S5 shows the distribution of the energy gaps, $P_i(X)$, for the initial and final states of azurin at 300 K.

We have also calculated the energy gaps produced by the protein part of thermal bath. The corresponding distributions are shown in Figure S6. The reorganization energies for the protein are listed in table S5.

The reorganization energies listed in Table S5 are calculated from variances of the energy gap in two electron-transfer states

$$\sigma_{X,i}^2 = 2k_{\mathrm{B}}T\lambda_i \qquad \text{(S6)}$$

Alternatively, the Stokes-shift reorganization energy is given in terms of average values of the energy gap in two

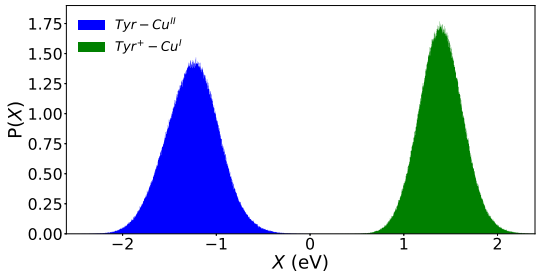

Figure S5. Distributions of the energy gap for $\mathrm{Tyr}^+ - \mathrm{Cu}^{\mathrm{I}}$ (green) and $\mathrm{Tyr} - \mathrm{Cu}^{\mathrm{II}}$ (blue) states at 300 K.

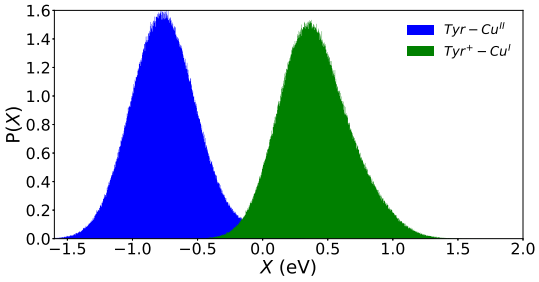

Figure S6. Distributions of the energy gap produced for the protein component for $\mathrm{Tyr}^+ - \mathrm{Cu}^{\mathrm{I}}$ (green) and $\mathrm{Tyr} - \mathrm{Cu}^{\mathrm{II}}$ (blue) states at 300 K.

states

$$\lambda^{\mathrm{St}} = \tfrac{1}{2}\left(\langle X\rangle_1 - \langle X\rangle_2\right) \qquad \text{(S7)}$$

The convergence of the reorganization energies λ as a function of the trajectory length is shown in Figure S7.

We have additionally performed a single umbrella sampling simulation[10? ?] at the intermediate state of the system between the final and initial electron transfer states and characterized by the Hamiltonian $H_z = H_1 + z(H_2 - H_1)$ at $z = 1/2$. The corresponding distribution of the energy gap is shown by the red line in Fig. S8.

V. CROSSOVER PARAMETER g

The dynamic crossover parameter g is calculated from the following equation[11]

$$g = \frac{2\pi V_e^2 \tau_x}{\sigma_X \hbar} \frac{e^{\frac{3}{2}\gamma^2\langle(\delta R)^2\rangle}}{\sqrt{2\beta\Delta F^\dagger + 4(\tau_x/\tau_R)\gamma^2\langle(\delta R)^2\rangle}} \qquad \text{(S8)}$$

Table S5. Reorganization energies of (eV) for the entire water-protein system and protein alone.

State	λ^{St}	λ_i	λ^{St}	λ_i
	Total		Protein	
$\mathrm{Tyr}^+ - \mathrm{Cu}^{\mathrm{I}}$	1.32	1.08	0.58	1.46
$\mathrm{Tyr} - \mathrm{Cu}^{\mathrm{II}}$	–	1.57		1.35

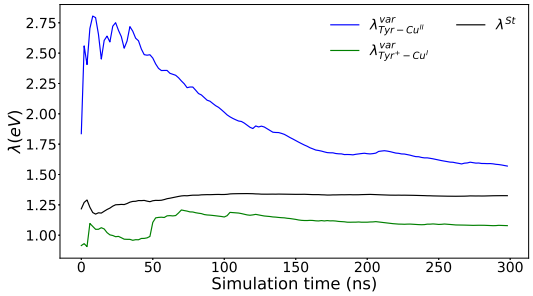

Figure S7. Running averages for the Stokes shift (Eq. (S7)) and variance reorganization energies (Eq. (S6)) in $\mathrm{Tyr}^+ - \mathrm{Cu}^{\mathrm{I}}$ (green) and $\mathrm{Tyr} - \mathrm{Cu}^{\mathrm{II}}$ (blue) states at 300 K.

in which the index specifying the state $i = 1, 2$ is dropped for brevity. All parameters required for the calculation of g are listed in Table S6. The value of the reaction free energy ΔF_0 is calculated from the difference of the reduction potentials of azurin and tyrosine as discussed in the main text.

The parameter γ in Eq. (S8) is the exponential decay of the electronic coupling

$$V(R) = V_{e,i} e^{-\frac{1}{2}\gamma \delta R}, \quad \delta R = R - R_{e,i} \tag{S9}$$

which is defined in terms of the equilibrium donor-acceptor distance $R_{e,i} = \langle R \rangle_i$ (Table S4) and the equilibrium coupling $V_{e,i} = V(R_{e,i})$. The distance dependence of electronic coupling is calculated using Voityuk's function[12]

$$\log_{10} V_e(R) = 1.73 - 0.42R \tag{S10}$$

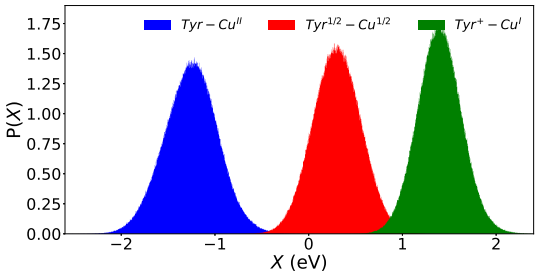

Figure S8. Distributions of the energy gap for $\mathrm{Tyr}^+ - \mathrm{Cu}^{\mathrm{I}}$ (green), $\mathrm{Tyr} - \mathrm{Cu}^{\mathrm{II}}$ (blue) and intermediate (z=1/2, red) states at 300 K.

Table S6. List of parameters for calculations of the dynamic crossover parameter g. All energies are in eV and times are in ps. The reaction free energy $\Delta F_0 = -0.859$ eV and $\gamma = 1.934$ $\mathrm{Å}^{-1}$ (Eq. (S10)) are used in the calculations.

State	$V_{e,i}$	$\Delta F_i^{\dagger}$	$\tau_x^{(i)}$	$\tau_R^{(i)}$	$\langle(\delta R)^2\rangle_i$,Å^2	g_i
$\mathrm{Tyr}^+ - \mathrm{Cu}^{\mathrm{I}}$ (1)	4.57×10^{-3}	0.007	8.47	18.25	0.10	11
$\mathrm{Tyr} - \mathrm{Cu}^{\mathrm{II}a}$ (2)	12.7×10^{-3}	1.05	10.39	57.98	0.43	70

In equation (S10), R is the distance between the centers of the donor and acceptor.

VI. Q-MODEL OF PROTEIN ELECTRON TRANSFER

The free energy surfaces of electron transfer $F_i(X)$ are specified in the Q-model[10,13] by the following equation

$$F_1(X) = \left(\sqrt{|\alpha||X - X_0|} - \sqrt{\alpha^2 \lambda_1}\right)^2$$
$$F_2(X) = \Delta F_0 + \left(\sqrt{|1+\alpha||X - X_0|} - \sqrt{(1+\alpha)^2 \lambda_2}\right)^2 \tag{S11}$$

in which the parameter X_0 defines the "fluctuation boundary" beyond which the reaction coordinate is not allowed to exist. This implies that $F(X < X_0) \to \infty$ at $\alpha > 0$ and $F(X > X_0) \to \infty$ at $\alpha < 0$. The parameter α specifies the extent of non-parabolicity of the free energy surfaces: $\alpha \to \infty$ restores the picture of crossing parabolas[14] and the range $-1 < \alpha < 0$ is not allowed. The fluctuation boundary X_0 is defined in terms of other parameters of the model by the following equation

$$X_0 = \Delta F_0 - \lambda_1 \frac{\alpha^2}{1+\alpha} \tag{S12}$$

The parameters α is specified in terms of two variance reorganization energies λ_i (Eq. (S6)) and the Stokes-shift reorganization energy (Eq. (S7)) as follows (Table S5)

$$\alpha = \frac{2\lambda^{\mathrm{St}} + \lambda_2}{\lambda_1 - \lambda_2} \tag{S13}$$

The consistency of calculations is tested by the identity imposed by the model

$$\zeta = \frac{\lambda_1 \alpha^3}{\lambda_2 (1+\alpha)^3} = 1 \tag{S14}$$

The parameters listed in Table S5 result in $\alpha = -8.6$ and $\zeta = 1.0042$.

The free energy surfaces presented in the main text are based on $\Delta F_0 = -1.04$ eV based on the reduction potential of $\mathrm{Trp}^+/\mathrm{Trp}^{\cdot}$ in water. If the the reduction potential of 1.8 V is adopted for the hydrophobic protein environment,[?] the reaction free energy becomes $\Delta F_0 = -1.46$ eV. The free energy surfaces for this setup are shown in Figure S9.

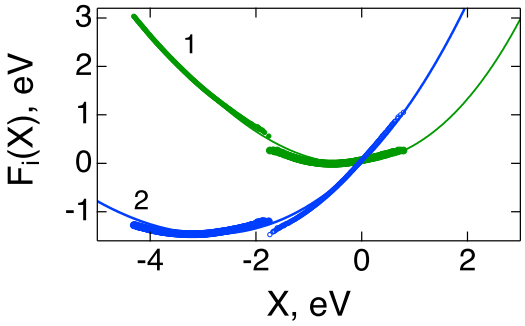

Figure S9. Free energy surfaces of electron transfer calculated in the Q-model (solid lines, see SM) and compared to MD simulations (filled points). The upper portions of the simulation data (open points) are obtained from the results around the minima by applying the linear relation (see the main text). The calculations are based on the estimated value of the reaction free energy $\Delta F_0 = -1.46$ eV.

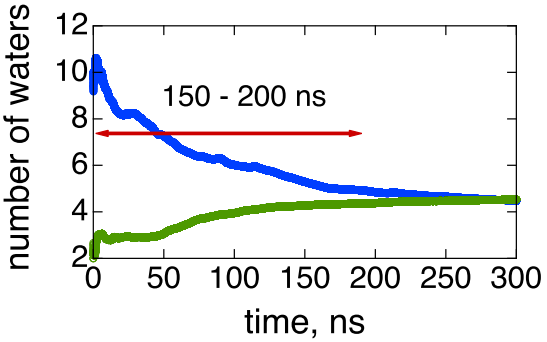

Figure S10. Cumulative average number of water molecules within a shell of 6 Å surrounding Tyr along 300 ns of MD trajectory for $\mathrm{Tyr} - \mathrm{Cu^{II}}$ (blue line) and $\mathrm{Tyr^{+}} - \mathrm{Cu^{I}}$ (green line). The horizontal arrow indicates the time scale on which the population of water molecules in around the Tyr residue relaxes.

VII. WETTING OF THE PROTEIN

To monitor the dynamics of wetting of the donor and acceptor cofactors, we calculated the average number of water molecules surrounding the tyrosine (Figure S10). Figure S11 shows water density maps near the tyrosine. Blue dots on the map refer to oxygen atoms of water molecules appearing within 6 Å cutoff during the last 30 ns of MD simulations. The pattern of wetting by hydration water is different for $\mathrm{Tyr^{+}} - \mathrm{Cu^{I}}$ and $\mathrm{Tyr} - \mathrm{Cu^{II}}$ states. This difference in the wetting pattern projects itself to unequal reorganization energies in two electron-transfer states as captured here by the Q-model.

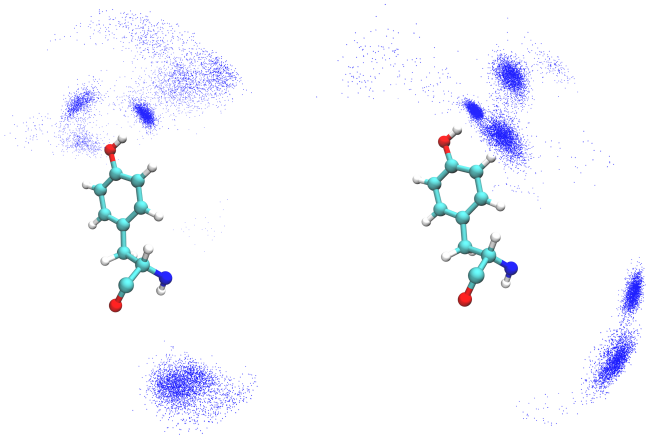

Figure S11. Water density maps within 6 Å cutoff from Tyr in the $\mathrm{Tyr} - \mathrm{Cu^{II}}$ state (left), in $\mathrm{Tyr^{+}} - \mathrm{Cu^{I}}$ (right).

REFERENCES

[1] S. M. Sarhangi and D. V. Matyushov, *J. Phys. Chem. B* (2022).

[2] W. Humphrey, A. Dalke, K. Schulten, *et al.*, *J. Molec. Graph.* **14**, 33 (1996).

[3] J. C. Phillips, R. Braun, W. Wang, J. Gumbart, E. Tajkhorshid, E. Villa, C. Chipot, R. D. Skeel, L. Kale, and K. Schulten, *J. Comput. Chem.* **26**, 1781 (2005).

[4] M. J. Frisch, G. W. Trucks, H. B. Schlegel, G. E. Scuseria, M. A. Robb, J. R. Cheeseman, G. Scalmani, V. Barone, G. A. Petersson, H. Nakatsuji, X. Li, M. Caricato, A. V. Marenich, J. Bloino, B. G. Janesko, R. Gomperts, B. Mennucci, H. P. Hratchian, J. V. Ortiz, A. F. Izmaylov, J. L. Sonnenberg, D. Williams-Young, F. Ding, F. Lipparini, F. Egidi, J. Goings, B. Peng, A. Petrone, T. Henderson, D. Ranasinghe, V. G. Zakrzewski, J. Gao, N. Rega, G. Zheng, W. Liang, M. Hada, M. Ehara, K. Toyota, R. Fukuda, J. Hasegawa, M. Ishida, T. Nakajima, Y. Honda, O. Kitao, H. Nakai, T. Vreven, K. Throssell, J. A. Montgomery, Jr., J. E. Peralta, F. Ogliaro, M. J. Bearpark, J. J. Heyd, E. N. Brothers, K. N. Kudin, V. N. Staroverov, T. A. Keith, R. Kobayashi, J. Normand, K. Raghavachari, A. P. Rendell, J. C. Burant, S. S. Iyengar, J. Tomasi, M. Cossi, J. M. Millam, M. Klene, C. Adamo, R. Cammi, J. W. Ochterski, R. L. Martin, K. Morokuma, O. Farkas, J. B. Foresman, and D. J. Fox, "Gaussian˜16 Revision C.01," (2016), gaussian Inc. Wallingford CT.

[5] B. Kaduk, T. Kowalczyk, and T. Van Voorhis, *Chem. Rev.* **112**, 321 (2012).

[6] C. M. Breneman and K. B. Wiberg, *J. Comput. Chem.* **11** (1990).

[7] Y. Shao, Z. Gan, E. Epifanovsky, A. T. Gilbert, M. Wormit, J. Kussmann, A. W. Lange, A. Behn, J. Deng, X. Feng, D. Ghosh, M. Goldey, P. R. Horn,

L. D. Jacobson, I. Kaliman, R. Z. Khaliullin, T. Kuś, A. Landau, J. Liu, E. I. Proynov, Y. M. Rhee, R. M. Richard, M. A. Rohrdanz, R. P. Steele, E. J. Sundstrom, H. L. W. III, P. M. Zimmerman, D. Zuev, B. Albrecht, E. Alguire, B. Austin, G. J. O. Beran, Y. A. Bernard, E. Berquist, K. Brandhorst, K. B. Bravaya, S. T. Brown, D. Casanova, C.-M. Chang, Y. Chen, S. H. Chien, K. D. Closser, D. L. Crittenden, M. Diedenhofen, R. A. D. Jr., H. Do, A. D. Dutoi, R. G. Edgar, S. Fatehi, L. Fusti-Molnar, A. Ghysels, A. Golubeva-Zadorozhnaya, J. Gomes, M. W. Hanson-Heine, P. H. Harbach, A. W. Hauser, E. G. Hohenstein, Z. C. Holden, T.-C. Jagau, H. Ji, B. Kaduk, K. Khistyaev, J. Kim, J. Kim, R. A. King, P. Klunzinger, D. Kosenkov, T. Kowalczyk, C. M. Krauter, K. U. Lao, A. D. Laurent, K. V. Lawler, S. V. Levchenko, C. Y. Lin, F. Liu, E. Livshits, R. C. Lochan, A. Luenser, P. Manohar, S. F. Manzer, S.-P. Mao, N. Mardirossian, A. V. Marenich, S. A. Maurer, N. J. Mayhall, E. Neuscamman, C. M. Oana, R. Olivares-Amaya, D. P. O'Neill, J. A. Parkhill, T. M. Perrine, R. Peverati, A. Prociuk, D. R. Rehn, E. Rosta, N. J. Russ, S. M. Sharada, S. Sharma, D. W. Small, A. Sodt, T. Stein, D. Stück, Y.-C. Su, A. J. Thom, T. Tsuchimochi, V. Vanovschi, L. Vogt, O. Vydrov, T. Wang, M. A. Watson, J. Wenzel, A. White, C. F. Williams, J. Yang, S. Yeganeh, S. R. Yost, Z.-Q. You, I. Y. Zhang, X. Zhang, Y. Zhao, B. R. Brooks, G. K. Chan, D. M. Chipman, C. J. Cramer, W. A. G. III, M. S. Gordon, W. J. Hehre, A. Klamt, H. F. S. III, M. W. Schmidt, C. D. Sherrill, D. G. Truhlar, A. Warshel, X. Xu, A. Aspuru-Guzik, R. Baer, A. T. Bell, N. A. Besley, J.-D. Chai, A. Dreuw, B. D. Dunietz, T. R. Furlani, S. R. Gwaltney, C.-P. Hsu, Y. Jung, J. Kong, D. S. Lambrecht, W. Liang, C. Ochsenfeld, V. A. Rassolov, L. V. Slipchenko, J. E. Subotnik, T. V. Voorhis, J. M. Herbert, A. I. Krylov, P. M. Gill, and M. Head-Gordon, *Mol. Phys.* **113**, 184 (2015), https://doi.org/10.1080/00268976.2014.952696.

[8] M. Dinpajooh, D. R. Martin, and D. V. Matyushov, *Sci. Rep.* **6**, 1 (2016).

[9] D. R. Martin, M. Dinpajooh, and D. V. Matyushov, *J. Phys. Chem. B* **123**, 10691 (2019).

[10] D. W. Small, D. V. Matyushov, and G. A. Voth, J. Am. Chem. Soc. **125**, 7470 (2003).

[11] D. V. Matyushov, J. Chem. Phys. **157**, 095102 (2022).

[12] A. A. Voityuk, *Chem. Phys. Lett.* **495**, 131 (2010).

[13] D. V. Matyushov and G. A. Voth, J. Chem. Phys. **113**, 5413 (2000).

[14] R. A. Marcus and N. Sutin, Biochim. Biophys. Acta **811**, 265 (1985).